Complexation and Toxicity of Copper in Higher Plants. II. Different Mechanisms for Copper versus Cadmium Detoxification in the Copper-Sensitive Cadmium/Zinc Hyperaccumulator *Thlaspi caerulescens* (Ganges Ecotype)[1][OA]

Ana Mijovilovich, Barbara Leitenmaier, Wolfram Meyer-Klaucke, Peter M.H. Kroneck, Birgit Götz, and Hendrik Küpper*

Department of Inorganic Chemistry and Catalysis, University of Utrecht, 3584 CA Utrecht, The Netherlands (A.M.); Universität Konstanz, Mathematisch-Naturwissenschaftliche Sektion, Fachbereich Biologie, D–78457 Konstanz, Germany (B.L., P.M.H.K., B.G., H.K.); EMBL Outstation Hamburg, Deutsches Elekronen-Synchrotron, D–22603 Hamburg, Germany (W.M.-K.); and Faculty of Biological Sciences and Institute of Physical Biology, University of South Bohemia, CZ–370 05 České Budejovice, Czech Republic (H.K.)

The cadmium/zinc hyperaccumulator *Thlaspi caerulescens* is sensitive toward copper (Cu) toxicity, which is a problem for phytoremediation of soils with mixed contamination. Cu levels in *T. caerulescens* grown with 10 μM Cu^{2+} remained in the nonaccumulator range (<50 ppm), and most individuals were as sensitive toward Cu as the related nonaccumulator *Thlaspi fendleri*. Obviously, hyperaccumulation and metal resistance are highly metal specific. Cu-induced inhibition of photosynthesis followed the "sun reaction" type of damage, with inhibition of the photosystem II reaction center charge separation and the water-splitting complex. A few individuals of *T. caerulescens* were more Cu resistant. Compared with Cu-sensitive individuals, they recovered faster from inhibition, at least partially by enhanced repair of chlorophyll-protein complexes but not by exclusion, since the content of Cu in their shoots was increased by about 25%. Extended x-ray absorption fine structure (EXAFS) measurements on frozen-hydrated leaf samples revealed that a large proportion of Cu in *T. caerulescens* is bound by sulfur ligands. This is in contrast to the known binding environment of cadmium and zinc in the same species, which is dominated by oxygen ligands. Clearly, hyperaccumulators detoxify hyperaccumulated metals differently compared with nonaccumulated metals. Furthermore, strong features in the Cu-EXAFS spectra ascribed to metal-metal contributions were found, in particular in the Cu-resistant specimens. Some of these features may be due to Cu binding to metallothioneins, but a larger proportion seems to result from biomineralization, most likely Cu(II) oxalate and Cu(II) oxides. Additional contributions in the EXAFS spectra indicate complexation of Cu(II) by the nonproteogenic amino acid nicotianamine, which has a very high affinity for Cu(II) as further characterized here.

Many heavy metals are well known to be essential microelements for plants, but elevated concentrations of these metals cause toxicity (for review, see Prasad and Hagemeyer, 1999; Küpper and Kroneck, 2005), as explained in more detail in our companion article (Küpper et al., 2009) on copper (Cu) complexation and toxicity in *Crassula helmsii*. Plants developed a number of strategies to resist this toxicity, including active efflux, sequestration, and binding of heavy metals inside the cells by strong ligands. Among the zinc (Zn) and cadmium (Cd) hyperaccumulators (Brooks, 1998; Lombi et al., 2000), the best known species is *Thlaspi caerulescens*, which has been proposed as a hyperaccumulator model species by several authors (Assunção et al., 2003; Peer et al., 2003, 2006). An enhanced uptake of metals into the root symplasm was found in *T. caerulescens* compared with the related nonaccumulator *Thlaspi arvense* (Lasat et al., 1996, 1998), and a reduced sequestration into the root vacuoles was associated with the higher root-to-shoot translocation efficiency of *T. caerulescens* (Shen et al., 1997; Lasat et al., 1998). This is likely related to elevated expression of xylem-loading transporters in the roots (Papoyan and Kochian, 2004; Weber et al., 2004). One of these, the Cd/Zn-pumping P_{1b}-type

[1] This work was supported by the Stiftung Umwelt und Wohnen and the Fonds der Chemischen Industrie (grant no. 661278 to H.K.), by the European Community Access to Research Infrastructure Action of the Improving Human Potential Programme to the EMBL Hamburg Outstation (contract no. HPRI–CT–1999–00017), and by Konstanz University (to H.K., P.M.H.K.).

* Corresponding author; e-mail hendrik.kuepper@uni-konstanz.de.

The author responsible for distribution of materials integral to the findings presented in this article in accordance with the policy described in the Instructions for Authors (www.plantphysiol.org) is: Hendrik Küpper (hendrik.kuepper@uni-konstanz.de).

[OA] Open Access articles can be viewed online without a subscription.

www.plantphysiol.org/cgi/doi/10.1104/pp.109.144675

ATPase TcHMA4, was recently purified as a protein, which revealed posttranslational processing, and its biochemical characterization showed Cd and Zn transport affinity in the submicromolar range (Parameswaran et al., 2007). Studies of cellular metal compartmentation have shown that in most hyperaccumulators, the metal is sequestered preferentially into compartments where it does no harm to the metabolism. These are, in most cases studied so far, the epidermal vacuoles (Küpper et al., 1999, 2001; Frey et al., 2000; Bidwell et al., 2004; Broadhurst et al., 2004), where concentrations of several hundred mmol L^{-1} can be reached in the large metal storage cells (Küpper et al., 1999, 2001). The latter showed that hyperaccumulation must be mediated by active pumping of the heavy metals into their storage sites, which was shown to be achieved by an extremely increased expression of metal transport proteins in leaves of hyperaccumulators compared with nonaccumulators (Pence et al., 2000; Assunção et al., 2001; Becher et al., 2004; Papoyan and Kochian, 2004; Küpper et al., 2007b). Strong sulfur (S) ligands like phytochelatins were shown not to be relevant for Cd detoxification in the Cd hyperaccumulator *T. caerulescens*. Phytochelatin levels are lower in this plant than in the related nonaccumulator *T. arvense* (Ebbs et al., 2002), inhibition of phytochelatin synthase in hyperaccumulators does not affect their Cd resistance (Schat et al., 2002), and direct measurements of the Cd ligands by EXAFS (Table I) showed that most of the Cd in this species is not bound by strong ligands but by weak oxygen (O) ligands (Küpper et al., 2004). Thus, the main detoxification strategy in hyperaccumulators is clearly not binding to strong ligands but sequestration of the hyperaccumulated heavy metals. However, the nonproteogenic amino acid nicotianamine (NA) seems to play an important role in metal homeostasis of plants. According to several studies, it binds iron, Zn, and Cu, mainly for long-distance transport in the vascular bundle (Stephan and Scholz, 1993; Pich et al., 1994; Schmidke and Stephan, 1995; Stephan et al., 1996, Pich and Scholz, 1996; von Wiren et al., 1999; Liao et al., 2000), and NA synthase has been shown to be highly overexpressed in hyperaccumulators compared with nonaccumulator plants (Becher et al., 2004; Weber et al., 2004; van de Mortel et al., 2006, 2008).

Under metal-induced stress, the heavy metal accumulation pattern changes. Under such conditions, heavy metal (Cd, nickel) accumulation was enhanced in a few cells of the mesophyll (Küpper et al., 2000a, 2001). The same cells contained elevated levels of magnesium, which was interpreted as a defense against

Table I. *Explanation of technical terms*

Technical Term	Explanation/Definition
Antenna connectivity	The likelihood of energy transfer between antennae of different photosystems (PSII and/or PSI)
DW	Debye-Waller factor of the EXAFS refinements, accounts for both structural and thermal disorder of the metal ion coordination shells (Binstead et al., 1992)
EF	Fermi energy of the EXAFS refinements, defines the threshold for the EXAFS spectra (Rehr and Albers, 2000)
EXAFS	Extended x-ray absorption fine structure
FI	Fit index of the EXAFS refinements = sum of the square of the residuals (this is what is minimized in the refinement)
F_0	Minimal fluorescence yield of a dark-adapted sample, fluorescence in nonactinic measuring light
F_m	Maximum fluorescence yield of a dark-adapted sample after supersaturating irradiation pulse
F_m'	Maximum fluorescence yield of a light-adapted sample after supersaturating irradiation pulse
F_p	Fluorescence yield at the P level of the induction curve after the onset of actinic light exposure
$F_v = F_m - F_0$	Variable fluorescence
$F_v/F_m = (F_m - F_0)/F_m$	Maximal dark-adapted quantum yield of PSII photochemistry
$\Phi_{PSII} = \Phi e = (F_m' - F_t')/F_m'$	The light-acclimated efficiency of PSII (Genty et al., 1989). In this article, the use of this parameter is extended to the relaxation period after the end of actinic light to analyze the return of the system to its dark-acclimated state as measured by F_v/F_m.
k	Wave number of the photoelectron, proportional to the square of the energy difference from the threshold energy (Efermi)
k-range	Energy range above the x-ray absorption edge of the metal where EXAFS was analyzed.
Light saturation	Measured by the increased amplitude of F_p relative to F_m after subtraction of F_0. $(F_p - F_0)/(F_m - F_0)$ is mostly dependent on the ratio of functional antenna molecules to functional reaction centers and electron transport chains. Under constant actinic irradiance for measuring F_p, a large antenna capturing photons and delivering them to its reaction center will cause more of the "electron traffic jam" that leads to F_p than a small antenna.
Multiple scattering	Contributions in EXAFS that originate not from direct interaction between the central ion and another atom, but from interactions between the different atoms of a ligand molecule. This can only be observed in very rigid (parts of) ligand molecules, e.g. the imidazole ring of His. Further, the contribution is most significant for forward scattering at angles close to 180°, which is the case for the atoms in an imidazole ring.
$NPQ = (F_m - F_m')/F_m$	Nonphotochemical quenching, in this article used as an acronym for the name of this phenomenon. In this article, we measure nonphotochemical quenching as q_{CN} = "complete nonphotochemical quenching of Chl fluorescence", i.e. with normalization to F_m.
Z	Atomic number

substitution of Mg^{2+} in chlorophyll (Chl; Küpper et al., 1996, 1998, 2002) by heavy metals. Recently, it was found that this heterogeneity of Cd accumulation is a transient phenomenon in *T. caerulescens* under Cd-toxicity stress, correlating with a heterogeneity in photosynthesis and disappearing when the plants acclimate to the stress (Küpper et al., 2007a). It was postulated that this transient heterogeneity constitutes an emergency defense against Cd toxicity by sacrificing a few mesophyll cells as additional storage sites until the metal sequestration in the epidermis is sufficiently up-regulated. Furthermore, this acclimation response showed that at least part of the Cd resistance of *T. caerulescens* is inducible (Küpper et al., 2007a).

While Cd resistance of *T. caerulescens* is strongly enhanced compared with related nonaccumulator plants, *T. caerulescens* is known to be sensitive to Cu to a similar extent as nonaccumulator plants, limiting its application for phytoremediating soils with mixed contamination (Walker and Bernal, 2004; Benzarti et al., 2008).

In contrast to other metals, the speciation (redox state and coordination) of Cu in plant tissues is poorly understood, despite the detailed structural and functional knowledge about numerous Cu-dependent enzymes and Cu chaperones (for review, see Pilon et al., 2006). This is most likely due to the difficulty of measuring Cu speciation. The concentrations of Cu in plant tissue are too small for NMR and were too small for EXAFS for a long time. Methods relying on fractionation or homogenization of fresh tissues (e.g. for chromatography) cause breaking of intracellular membranes. This brings weakly bound metal that was localized in the vacuole into contact with the various strong ligands of the cytoplasm, causing artifactual changes of speciation. To our knowledge, so far only one EXAFS study on Cu speciation in plant tissues used environmental Cu concentrations: Polette et al. (2000) studied Cu speciation in the Cu-resistant Cu indicator plant *Larrea tridentata*. In their EXAFS measurements on samples frozen in liquid nitrogen, they found evidence for a Cu(II)-phytochelatin complex involved in transport and an unknown Cu complex involved in Cu storage. A second study using the same sample preparation method (that due to the formation of a gas layer around the sample slows freezing, resulting in ice formation with the risk of membrane damage) investigated the Cu-tolerant Cu-excluder plant *Elsholtzia splendens* (Shi et al., 2008). Unfortunately, these authors applied very high, physiologically not relevant Cu levels (300 μM) in their nutrient solution in order to force enough Cu into the tissues to get an acceptable signal-noise level in their EXAFS data within the limited synchrotron beam time. In two further Cu-EXAFS studies on plant tissues (Gardea-Torresdey et al., 2001, on *L. tridentata*; Sahi et al., 2007, on *Sesbania drummondii*), strong artifacts were most likely introduced by drying of tissues. Drying disrupts membranes as discussed above and can remove aquo ligands from metal ions (Schünemann et al., 1999). Additionally, extremely high Cu concentrations in the nutrient solution were applied to the plants (1,000 and 10,000 μM by Gardea-Torresdey et al., 2001; 400–5,000 μM by Sahi et al., 2007). Thus, the biological relevance of these studies has to be questioned.

In this study, we addressed two related questions, both in comparison with the Cu accumulator *C. helmsii* described by Küpper et al. (2009). How do environmentally relevant (10 μM) toxic levels of Cu affect *T. caerulescens*? And how does the plant try to defend itself by binding the Cu ions? This was done by investigating mechanisms of Cu-induced inhibition of photosynthesis and analyzing the complexation of Cu in leaves. The latter was done in order to find out whether *T. caerulescens* utilizes different mechanisms for detoxification of the nonaccumulated Cu in comparison with the hyperaccumulated Cd. The speciation of Cu was analyzed by EXAFS, which is an element-specific method and therefore particularly suited for analyzing the in vivo ligand environment of metals in plants. Furthermore, in contrast to most other methods, it is applicable to intact frozen-hydrated plant tissues, which were first used by Salt et al. (1995). Moreover, EXAFS beamlines can now reach much lower metal concentrations than heteronuclear NMR (Ascone et al., 2003). So far, metal NMR was applied only in the case of Cd in *T. caerulescens* (Ueno et al., 2005), but although the concentration of this hyperaccumulated metal in the tissue was about 100 times higher than that of Cu, the NMR signal obtained was so weak that only the most abundant ligand type (organic acids, confirming previous EXAFS work [Küpper et al. 2004]) could be detected; everything else was drowned in noise. Thus, EXAFS is the method of choice for identifying ligands of both Cu(I) and Cu(II) in intact tissues in the absence of artifacts introduced by sample preparation (see above). EXAFS model complexes were prepared as references, and among these, Cu(II)-NA was characterized in more detail by UV/VIS and electron paramagnetic resonance (EPR) spectroscopy in view of its importance for Cu(II) binding in *T. caerulescens*. Inhibition of photosynthesis was investigated, as in our *C. helmsii* study, by the two-dimensional (imaging) microscopic in vivo measurement of the transients of Chl variable fluorescence with a recently described instrument, the fluorescence kinetic microscope (FKM; Küpper et al., 2007a). This was complemented with data on Cu accumulation, changes in pigment composition, and plant growth.

RESULTS

Plant Growth and Metal Uptake, Visual Symptoms of Cu Stress

There was little difference in growth inhibition by Cu between the Cd/Zn hyperaccumulator *T. caerulescens* and the related Cd/Zn nonaccumulator (possible Ni

Table II. *Plant growth and Cu concentrations in the plant samples*
The values are means ± SE of three to 10 plants. –, Not determined.

Sample	Cu in the EXAFS Samples, *n* = No. of Plants Used for EXAFS	Plant Fresh Weight after 8 Weeks of Growth, *n* = No. of Plants Used for Fresh Weight	Plant Fresh Weight after 4 Months of Growth, *n* = No. of Plants Used for Fresh Weight
	mg kg^{-1} dry wt	*g*	*g*
T. caerulescens, 0.1 μM Cu^{2+}	–	5.31 ± 1.60, *n* = 4	54.7 ± 4.6, *n* = 6
T. caerulescens, 10 μM Cu^{2+}, resistant individuals	42.7 ± 8.1, *n* = 5	–	6.33 ± 1.31, *n* = 3
T. caerulescens, 10 μM Cu^{2+}, sensitive individuals	34.4 ± 3.8, *n* = 8	0.043 ± 0.041, *n* = 4	2.08 ± 0.17, *n* = 10
T. fendleri, 0.1 μM Cu^{2+}	–	2.66 ± 1.06, *n* = 4	–
T. fendleri, 10 μM Cu^{2+}	–	0.04 ± 0.042, *n* = 4	–

accumulator) *Thlaspi fendleri*. At 10 μM Cu^{2+} for 8 weeks, fresh weight of *T. caerulescens* was reduced to 1% of the control and that of *T. fendleri* to 1.5% (Table II). Remarkably, in this case the hyperaccumulator *T. caerulescens* was even slightly more sensitive than the nonaccumulator *T. fendleri*. A few individuals of *T. caerulescens*, however, turned out to be much more Cu resistant, which became obvious mainly after a longer time of growth, indicating acclimation. After 3 to 4 months of growth, the Cu-resistant individuals had, on average, about three times higher fresh weight compared with the regular sensitive individuals (Table II). This was not related, however, to some physiological metal exclusion mechanism, less supply of nutrient solution to the pots (as resistant and nonresistant plants were growing in the same pots), or any other effect reducing Cu load in the shoots. Surprisingly, the Cu content in leaves of the resistant individuals was even 25% higher than in leaves of sensitive individuals (Table II). Nevertheless, the Cu contents in all *T. caerulescens* leaves were typical for nonaccumulator plants (less than 50 ppm). The resistant individuals looked much healthier in terms of the number and size of living leaves, but also they had slightly chlorotic leaves (Fig. 1 shows one of the most Cu-resistant individuals we observed).

Some of the Cu-stressed plants stayed green, and others became partially chlorotic. The first case was correlated with the occurrence of some [Cu(II)]-Chl *a* in extracts of the plants, although the [Cu(II)]-Chl content never exceeded 2% of total Chl. This and the bleached plants showed that the type of damage in these plants was closer to the "sun reaction" (characterized by heavy metal insertion only in the PSII reaction center) than to the "shade reaction" (characterized by the formation of heavy metal substituted Chls in the light-harvesting complex II [LHCII] antenna of PSII; Küpper et al., 2002). The bleaching in this case cannot be due to bleaching of [Cu(II)]-Chl, because this pigment is highly stable (Küpper et al., 1996).

Cu-Induced Inhibition of Photosynthesis

The biophysical meaning of the fluorescence kinetic parameters used in the following text is described in more detail in Table I; an introduction to the subject is given in the review by Maxwell and Johnson (2000). Cu stress in *T. caerulescens* decreased the maximal dark-adapted quantum yield of PSII photochemistry, $F_v/F_m = (F_m - F_0)/F_m$, as well as the light-acclimated efficiency of electron transport through PSII, $\Phi_{PSII} = (F_m' - F_t')/F_m'$ (Fig. 2). This was caused by a dramatic increase in the basic fluorescence yield, F_0, that was stronger than the increase of the maximal fluorescence yield, F_m. While Cu toxicity increased F_0 slightly more (410% instead of 360%) in the Cu-sensitive than in the Cu-resistant individuals, F_m increased more (about

Figure 1. Visual differences after growth in hydroponic solution for 4.5 months. Top, Two plants stressed in the same pot with 10 μM Cu^{2+}, showing the difference in growth between a Cu-sensitive (left) and a Cu-resistant (right) individual of *T. caerulescens* (Ganges population). Bottom, Control plant grown at 0.1 μM Cu^{2+}.

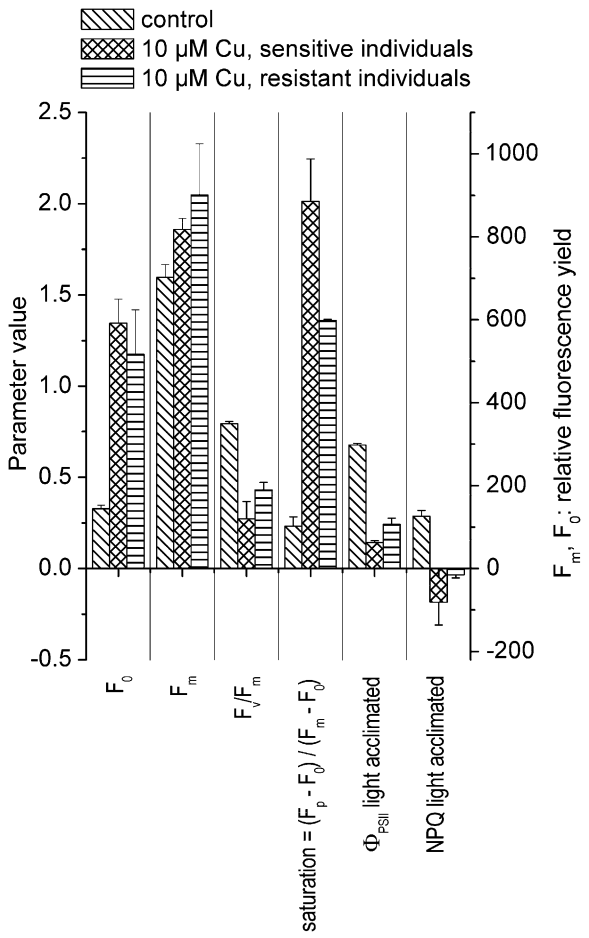

Figure 2. Fluorescence kinetic microscopy of Cu-stressed *T. caerulescens*. The data are from a typical experiment from the second series of experiments (see "Materials and Methods"), the same experiment used for Figure 3 of our publication about Cd acclimation (Küpper et al., 2007a), so that the controls were the same and the effects of Cu (reported now) and Cd (reported before) are directly comparable. Actinic irradiance during measurement was about 40 μmol m^{-2} s^{-1}. Averages and SE values of all measurements between 3 and 5 weeks of treatment with Cu are shown. The meaning of the fluorescence kinetic parameters is explained in Table I.

20% instead of 10%) in the latter. Based on the above-mentioned definitions, this led to a milder decrease of F_v/F_m and Φ_{PSII} in the Cu-resistant compared with the Cu-sensitive specimens. The values of nonphotochemical quenching of excitation energy, measured as NPQ = $(F_m - F_m')/F_m$, became negative under Cu stress (i.e. more excited states of Chl relaxed via fluorescence in the light-adapted compared with the dark-adapted state of the photosynthetic system). In the Cu-sensitive individuals, these negative NPQ values were of similar amplitude as the positive NPQ values in the control. In the Cu-resistant individuals, NPQ was almost zero. The light saturation of the photosynthetic system, measured as $(F_p - F_0)/(F_m - F_0)$ as described before (Küpper et al., 2007a), was very strongly affected by Cu. Light saturation of the Cu-stressed plants was about 2 for the sensitive and 1.4 for the resistant Cu-stressed plants, which means that the maximal fluorescence quantum yield after the onset of actinic light (F_p) was higher than the normally highest maximum fluorescence quantum yield, which is measured in the dark-adapted state (F_m). In contrast, light saturation was only 0.25 for the controls (Fig. 2).

Characterization of Cu Ligands by EXAFS, EPR, and UV/VIS Spectroscopy

As in our previous EXAFS studies, including the companion article (Küpper et al., 2009) on *C. helmsii*, we characterized several Cu complexes in solution. They served as a basis for evaluating the EXAFS spectra of plant samples, where many ligands could contribute to Cu ligation. These model complexes were selected because they are likely Cu ligands themselves [Cu(II)-His and Cu(II)-NA] or because they could be used as simplified models of complex ligands in vivo (glutathione as a first shell ligand model for the various S ligands in plants).

Cu(II)-His

A fit of its EXAFS spectrum with four His residues bound by the imidazole nitrogen had the best fit index (FI), but the Debye-Waller factors (DW) of the higher shells were rather high, indicating larger than expected disorder in those ligand shells. Thus, fits with lower coordination of His and addition of a low-Z ligand (O) were tried. The best combination of FI and DW parameters was found for two His residues (bound by the imidazole nitrogen) and two O, while 6-coordination models resulted in unrealistically higher DW parameters (Fig. 3).

Cu(II)-Pro

In the case of Cu(II)-Pro, the best fit was for 4-coordination of low-Z ligands (O was used). The higher shell contributions could not be fitted with imidazole rings (emulating the Pro ring structure), which may indicate that Pro was bound not by the ring but by the carboxylate end.

Cu(I/II)-Glutathione

This was a mixture of the Cu(I) and Cu(II) complex as generated by the preparation method. Its EXAFS spectrum (Fig. 3) was modeled with the Cu site coordinated to four S atoms in the first shell. A second shell of carbon (C) led to higher FI than a Cu-Cu interaction at about 2.7 Å. For a mixed first shell with S and low-Z ligands (O was tried), the best fit was found for three S and one O and a Cu-Cu interaction in the higher shell. However, this model was discarded

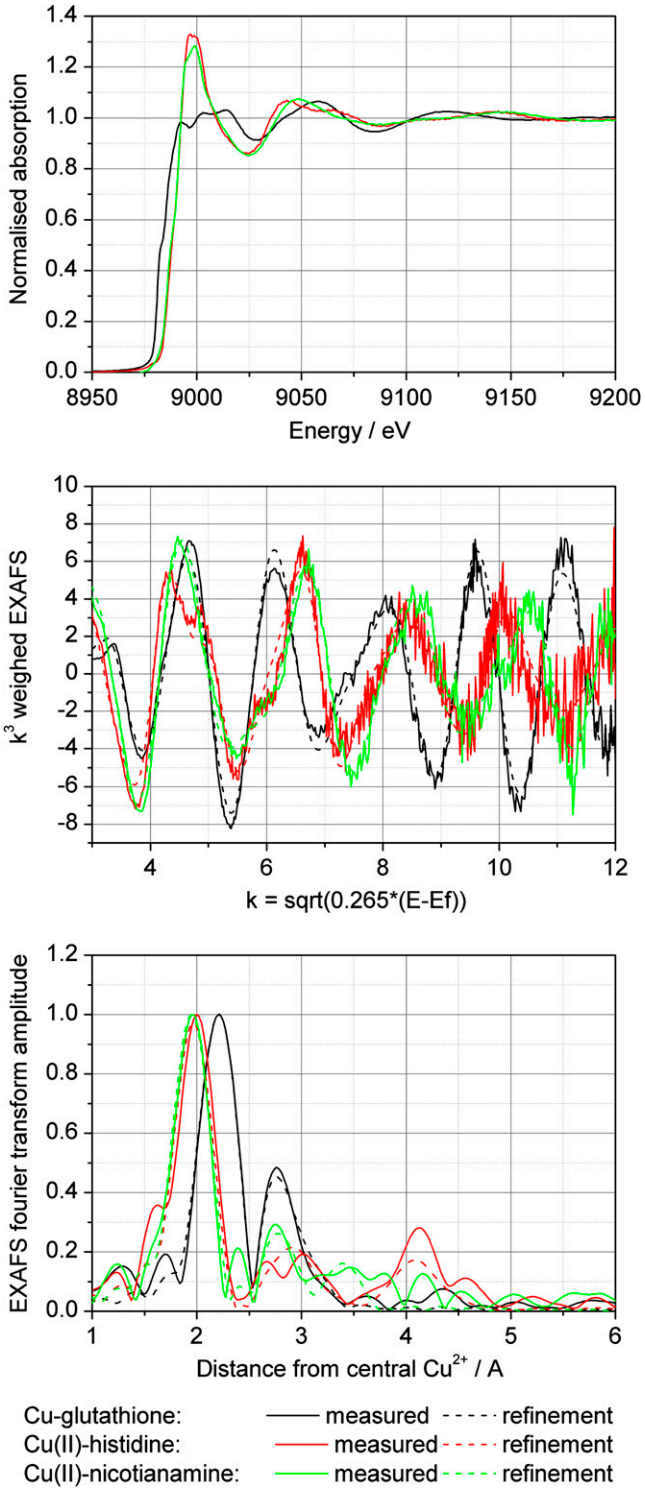

Figure 3. Comparison of Cu x-ray absorption spectra of different model compounds. Top, Raw data after normalization. Note that x-ray absorbance was measured as an excitation spectrum of x-ray fluorescence. Middle, Normalized EXAFS. Bottom, Fourier transform of the EXAFS.

because of the very long (unrealistic) distance obtained for the bound O. The DW parameter found for O was small for a 4-coordinated Cu complex, suggesting that the coordination number might be higher. However, increasing the coordination to 5 by adding one more O led to a negative DW parameter for that O. In summary, the most realistic model consists of a CuS_4 center and a Cu-Cu interaction due to the formation of a cluster with two Cu bridged by S, plus coordination of each Cu by another two S from glutathione (i.e. Cu_2GS_6).

Cu(II)-NA

The EXAFS results were similar for both pH values analyzed (pH 4 and 7). For modeling the structure of NA in the refinements, we used the mugeinic acid structure published by Nomoto et al. (1981), because both molecules are almost identical. For both NA samples, the fits including four ligands in the first shell and two additional long ligands gave a rather high DW parameter for the long ligands. The improvement in the FI was tiny, which with an increased number of parameters reduces the significance of the additional ligands. Therefore, the EXAFS result alone was not sufficient to decide whether the Cu(II) bound to NA was 4- or 6-coordinated. However, it is well in agreement with a 6-coordinated model where two highly mobile water molecules are bound at longer distances (Table III; Fig. 3).

In order to obtain a more definite answer about the coordination of Cu in the Cu(II)-NA complex, EPR spectroscopy was applied. At X-band, 20 K, Cu(II)-NA exhibited a rather simple close to isotropic signal over the range pH 3 to 7, with a baseline crossing at g-factor $\approx$ 2.12 (Fig. 4B). The signal kept its shape independent of temperature (5–70 K) and concentration of Cu (0.43–0.10 mM). Cu(II)-NA was fully EPR active under our experimental conditions, as documented by double integration of the signal, and there were no transitions detectable at half-field indicative for Cu-Cu interaction. Overall, the EPR properties of Cu(II)-NA are in line with a hexadentate complex, similar in structure to the related Cu(II)-mugineic acid complex whose three-dimensional structure has been obtained by x-ray crystallography (Nomoto et al., 1981). NA provides six alternating carboxylate and amine functions whose relative positions favor the formation of 6-coordinated metal complexes as discussed recently (Callahan et al., 2006).

The UV/VIS absorption spectra of NA showed an absorption maximum at 272 nm (Fig. 4A). Addition of Cu^{2+} at pH values above 2 caused a pronounced shift of the maximum to 247 nm and a very strong increase in intensity of this band. Furthermore, a weak additional absorption maximum appeared at 609 nm ($\varepsilon_{609} \approx 100\ M^{-1}cm^{-1}$). At pH 2, the spectrum of the NA+Cu^{2+} mixture already had a shape intermediate between the spectrum of NA alone and that of the Cu (II)-NA complex at higher pH values: it had a low peak at 247 nm and a residual shoulder at 272 nm. Also, the 609-nm absorption peak started to appear at pH 2 (Fig. 4A).

Table III. *Results of the refinement (explanation with a theoretical model) of the EXAFS spectra of model compounds using the DL-Excurve program*

The graphs of the fits for Cu(I/II)-glutathione, Cu(II)-His, and Cu(II)-NA at pH 7 are shown in Figure 3. The refinements of model compounds that were more relevant for *C. helmsii* [aqueous Cu(II), Cu(II)-citrate, and Cu(II)-malate] are shown in the companion article (Küpper et al., 2009) about Cu metabolism in that species. EF, Fermi energy, defines the threshold for the EXAFS spectra (Rehr and Albers, 2000; this value was refined for every sample); FI, fit index, increases with decreasing quality of the fit; SE, mathematical SE values of the refinement (2σ level). The error of the EXAFS approach as such is higher; this is revealed by the differences between samples of the same type. Asterisks indicate values that were constrained to be identical for these contributions. Deviations from this simplification do not improve the model significantly.

Sample	No., Type of Ligands per Shell ± SE	Distance ± SE	$2\sigma_i^2 \pm 2\sigma$ SD	EF ± SE	FI (No. of Variables)
		Å	Å^2		
Cu-glutathione[a]	3.6 ± 0.2, S	2.260 ± 0.002	0.006 ± 0.001	−11.5 ± 0.4	0.142
	4.5 ± 0.6, Cu	2.710 ± 0.005	0.021 ± 0.002		
Cu(II)-His	5.0 ± 0.8, N[b]	2.000 ± 0.006*	0.008 ± 0.001*	−10.5 ± 0.6	0.403
	0.4 ± 0.8, O	2.000 ± 0.006*	0.008 ± 0.001*		
Cu(II)-NA, pH 4	3.8 ± 0.3, N/O	1.980 ± 0.003	0.009 ± 0.001	−9.8 ± 0.4	0.251
	3.7 ± 0.8, C	2.862 ± 0.012	0.011 ± 0.004*		
	5.0 ± 1.3, C	3.403 ± 0.015	0.011 ± 0.004*		
Cu(II)-NA, pH 7	5.6 ± 0.3, N/O	1.975 ± 0.003	0.006 ± 0.001	−9.4 ± 0.5	0.305
	4.1 ± 0.8, C	2.837 ± 0.010	0.006 ± 0.003*		
	4.7 ±1.2, C	3.394 ± 0.014	0.006 ± 0.003*		
Cu(II)-Pro, pH 7	5.2 ± 0.3, N/O	1.957 ± 0.004	0.008 ± 0.001	−12.5 ± 0.5	0.285

[a]Mixture of Cu(I) and Cu(II) as obtained by the preparation method. [b]Bound to His.

EXAFS Spectroscopy of Plant Samples

In contrast to typical EXAFS spectra of metals in biological systems, here more than a single contribution (or metal-to-neighbor atom distance) could be identified, which was visualized by corresponding peaks in the Fourier transforms. Generally, the EXAFS spectra of all plant samples had a much higher noise and therefore worse statistics, in particular in the high k-range (i.e. high above the Cu absorption edge), compared with the model compounds (Fig. 5). This noise level was inevitable because *T. caerulescens* is not a Cu hyperaccumulator (see atomic absorption spectrometry data), and environmentally relevant Cu concentrations have been used for plant growth. Therefore, we had to measure each sample for about 3 d until the statistics were sufficient for detailed analysis. Thus, the current set of data, consisting of eight plant samples, amounted to almost a month of EXAFS beamtime. For getting a further reduction of the noise to half, four times more integration time (12 d per sample) would have been needed, which would have been impossible at any synchrotron beamline. Like the refinements, the component analysis also was limited by this noise level, but still it yielded reasonably reproducible data, as indicated by the error bars after averaging the data from independent plant samples (Fig. 6). As malate, citrate, and the aquo complex could not be distinguished from each other, their values in the fits are presented only as the sum of these three components.

For the first shell contributions in the refinements (Table IV), O/nitrogen (N) and S ligands were tested. For contributions from higher shells, NA was tested because it was previously predicted to play a role in Cu metabolism (Pich and Scholz, 1996; Liao et al., 2000; Irtelli et al., 2009). NA was fitted using the parameters (distances, ligand types, and numbers of individual ligand shells) of the model compound. As Cu(II)-NA is a metal:ligand 1:1 complex, this structure should not be different in the presence of other potential ligands. The overlap of the long first shell O ligands with possible S, Cu, or phosphorus (P) contributions was taken into account in the interpretation of the data. Interestingly, NA alone could not explain the high amplitude of the peak at 2.7 to 3 Å; tests of possible ligand atoms resulted in the conclusion that P, Cu, or S is most likely the second contributor to this peak. The contributions at above 3.3 Å could not be explained by NA, His, or any other of the tested model compounds. Various atom types were tested for each major contribution, resulting in the conclusion that these contributions show Cu-Cu interactions from rigid Cu clusters. It should be noted that this contribution is so dominant at higher k-values in the EXAFS that even at the present noise level the identification of these metal clusters is significant.

Besides these general observations, the following sample-specific characteristics of Cu ligation were found.

Cu-Resistant Plants, Young Leaves (Three Samples)

Cu was found to be 4-coordinated in the first ligand shell, with a mixture of O and S ligands. On average, 1.7 ± 0.2 S ligands were found. Furthermore, 2.2 ± 0.2

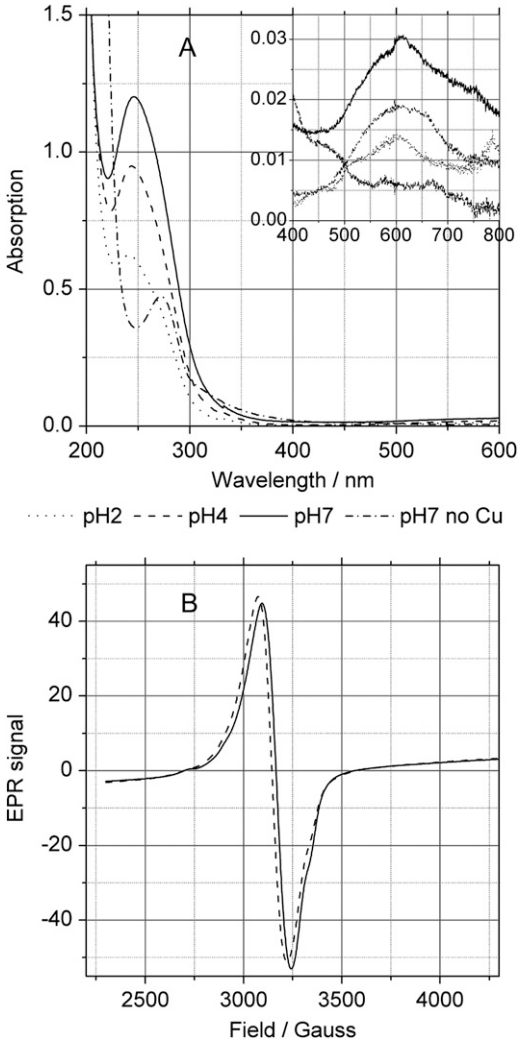

Figure 4. Optical and EPR spectra of Cu(II)-NA. A, UV/VIS absorption spectra of 0.4 mM NA or 0.4 mM NA with 0.32 mM Cu^{2+} ($CuCl_2$) in the short and long (inset) wavelength ranges. B, EPR spectra of the NA-Cu complex at pH 2 to 7.

O ligands were found in the first ligand shell, of which 1.6 ± 0.7 were ascribed to O ligands from NA carboxylates by the characteristic contribution at 2.8 Å (see model compound) that is not detectable in small organic acids like malate or citrate. In one of the samples, a fit with His instead of NA yielded a better DW parameter, probably because in this sample also the characteristic scattering of NA at 3 Å was less pronounced (data not shown). Besides NA, the 3-Å peak included contributions from P or S, fitted as 2.6 ± 0.3 P atoms in the refinements shown in Table IV. Furthermore, all of these samples showed a particularly intense peak in the Fourier transform at rather high distance (about 5.2 Å), which was best fitted by a Cu-Cu interaction with 4.5 ± 0.8 Cu at this distance from the central atom (Fig. 5). Also, the peaks between this and the 2.7- to 3-Å peak could only be explained by a heavy backscatterer like Cu. In summary, it can be clearly stated that O and S ligands contributed to the Cu binding in the first shell, and there is evidence for contributions from NA and Cu-Cu interactions. Possibly, His was involved as a ligand as well. This result was confirmed by the component analysis, where around 65% of the Cu ligands were found to be S, with the remainder being mainly His (Fig. 6).

Cu-Resistant Plants, Mature Leaves (Two Samples)

Similar results as for the young leaves were also obtained for the mature leaves. Again, 1.6 ± 0.4 S ligands and 2.2 ± 0.4 O ligands were detected in the first shell. The O ligands were almost all (2.1 ± 0.4) identified as NA by its characteristic contribution at about 2.8 Å (see above). In the best data set, a reasonable signal-noise ratio was available until k = 11.5 $Å^{-1}$. When using His as a ligand, the best fit was found for two His residues and two S bound to Cu. But also in this sample, the fit including NA instead of His gave a better picture, because this spectrum had a rather sharp peak at about 3 Å in its Fourier transform, which is characteristic for NA (see above). In the outer shells, again strong Cu-Cu contributions were found, with 3.1 ± 0.6 Cu at 5.2 Å from the central Cu atom. The component analysis supported the contribution of NA rather than His to Cu binding. Furthermore, it clearly showed a strong S contribution but slightly less S than in the young leaves (50% instead of 65%; Fig. 6).

In summary, it seems that also in mature (as in young) leaves of resistant individuals of *T. caerulescens*, Cu is mainly bound by a combination of S (thiolate) ligands and NA, with a noticeable shift from S ligands to NA coordination during leaf maturation. As in the mature leaves, the strong contributions at very large distances from the central Cu could be explained only by assuming a rigid cluster of Cu so that Cu-Cu contributions become visible in the EXAFS spectrum.

Cu-Sensitive Plants, Young and Mature Leaves (Three Samples)

For the first shell, the best refinement was obtained for 1 ± 0.3 S and 2.9 ± 0.4 O; of the O, 2.2 ± 0.9 were refined as NA. Like the S contribution in the first shell, also the S/P contribution at about 2.9 Å was less pronounced than in the Cu-resistant individuals: 0.7 ± 0.2 P were refined for the sensitive individuals compared with 1.9 ± 0.3 for the resistant individuals. As in the samples of the resistant plants, again there was a large peak at 5.2 Å in the Fourier transform that was ascribed to a Cu-Cu contribution. However, it was smaller than in the resistant plants; on average, 4 ± 0.8 Cu atoms were refined in the 5.2-Å peak in the Cu-resistant individuals, while 3.1 ± 0.3 Cu atoms were refined for this peak in the Cu-sensitive individuals. The component analysis again confirmed the refinements by yielding a mixture of S and O/N ligands but additionally showed better the contribution of NA (Fig. 6). While the proportion of Cu binding to NA was

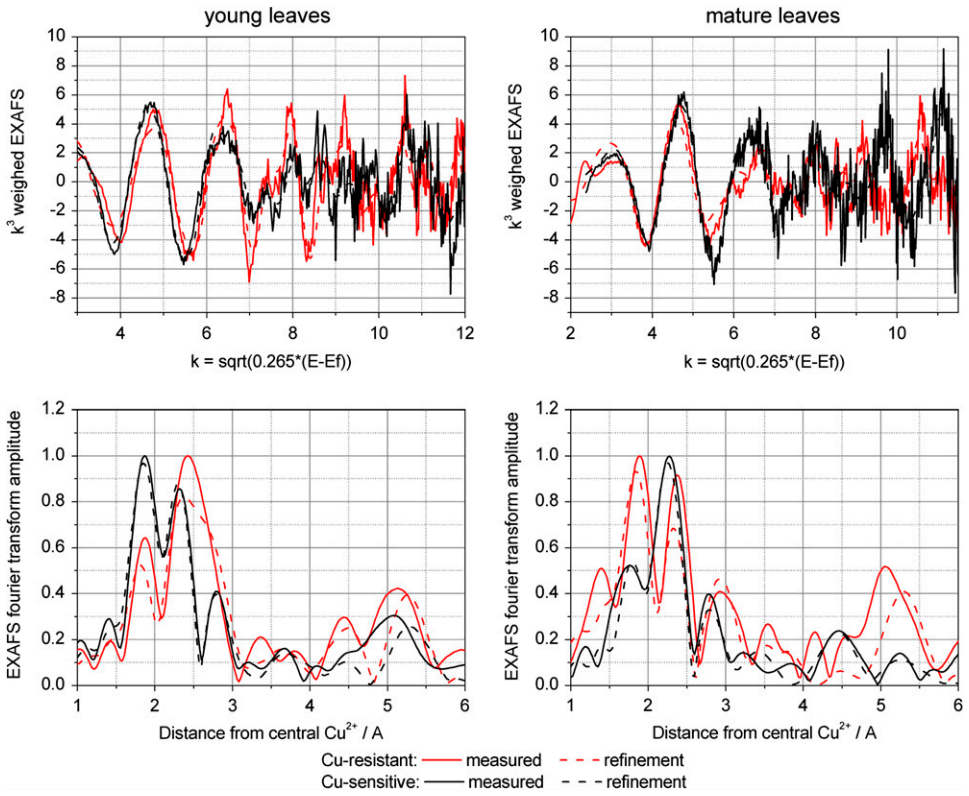

Figure 5. Typical examples of data obtained by in situ x-ray absorbance measurements (Cu-K edge) of frozen-hydrated *T. caerulescens* tissues. This example represents a measurement of Cu-EXAFS in a mature leaf of a Cu-resistant specimen. Top, Normalized EXAFS and fit with the theoretical model. Bottom, Fourier transform of the EXAFS and fit with the theoretical model (done on normalized EXAFS) as well as fit with data sets of model compounds.

similar as in the resistant individuals, the S contribution was clearly lower, and a rather strong contribution from hydrated ions and/or from organic acids such as malate or citrate was found instead.

DISCUSSION

Here, we analyzed the response of the Cd/Zn model hyperaccumulator *T. caerulescens* to the nonaccumulated metal Cu, to which this species is as sensitive as related nonaccumulator species. This sensitivity is important because it limits the application of *T. caerulescens* for the phytoremediation of soils with mixed contamination, as recently tested (Walker and Bernal, 2004). Our study has revealed that this may be due to the metal specificity of the metal detoxification system in *T. caerulescens*, since Cu was bound by completely different predominant ligands than Cd or Zn. This is particularly interesting because in our companion study (Küpper et al., 2009) on Cu metabolism in *C. helmsii*, we demonstrated that in this Cu-accumulating species this metal was bound to weak O ligands similar to the binding patterns for Cd and Zn in *T. caerulescens*. Furthermore, in this study, in all experiments a few individuals turned out to be somewhat more Cu resistant than others, and notably, those resistant individuals again had different Cu ligands.

In addition to new insights into the ligand environment of Cu in *T. caerulescens*, in our assessment of the vitality of the plants by measuring in vivo Chl fluorescence kinetics we found interesting aspects of the mode of inhibition by this metal. In particular, we observed an enhanced coupling of LHCII to PSII, most likely caused by Cu-induced inhibition of the water-splitting complex.

Physiological Effects of Cu on Sensitive and Resistant Individuals

As in our companion article (Küpper et al., 2009) on Cu effects in *C. helmsii*, in this study we investigated Cu stress under high-irradiance conditions or with long light phases, leading to the sun reaction type of damage to photosynthesis (Küpper et al., 1996, 1998, 2002) with an inhibition of the PSII reaction centers, like that due to the insertion of Cu^{2+} into the pheophytin *a* of the PSII reaction center (Küpper et al., 2002). The resulting decrease of F_v/F_m was observed also by Lanaras et al. (1993) with Cu-stressed *Triticum aestivum*. This decline resulted from an increase of the basic fluorescence yield F_0 and a decrease of the variable fluorescence yield F_v, in line with both our former studies and those of Lanaras et al. (1993). The same applies to the decline of the quantum yield of PSII photochemistry in the light-acclimated state as measured by the Φ_{PSII} parameter. The increase of F_0 despite the decreasing pigment content of the leaves looks surprising at first glance, but it was observed earlier (Ouzounidou et al., 1997; Küpper et al., 2007a) and is most likely caused by deeper penetration of exciting light and fluorescence emission from deeper

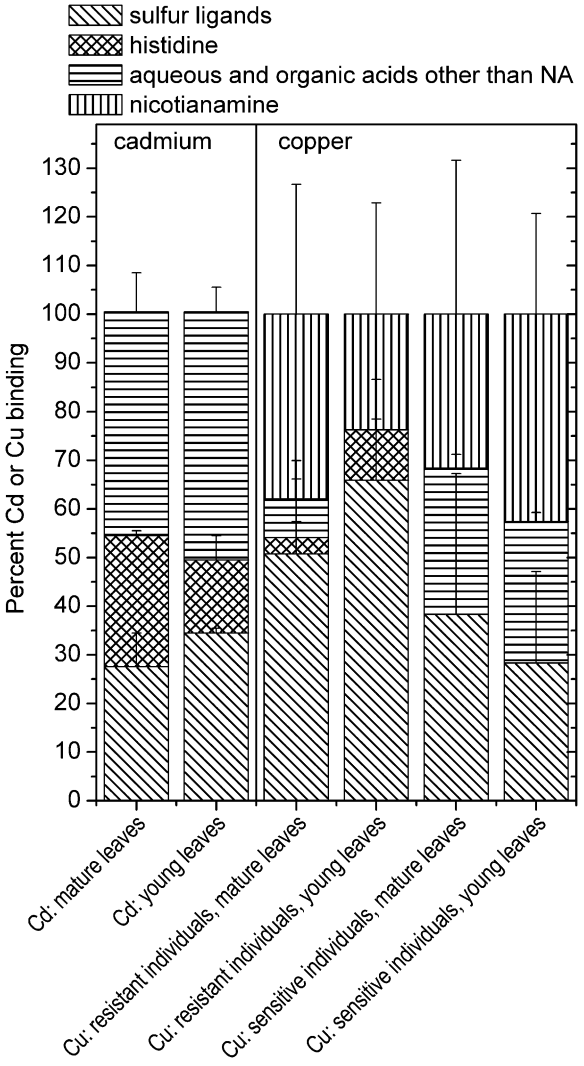

Figure 6. Metal-, age-, and specimen-dependent differences in ligand environment. Right, Averaged samples of leaves from plants grown on 10 μM Zn^{2+} and 10 μM Cu^{2+}: Cu-K edge (data from this study). Plant EXAFS spectra (k^3 weighed) were fitted with a linear combination of the EXAFS spectra of the following model compounds: aqueous ($CuSO_4$), Cu(II)-malate, Cu(II)-citrate, Cu(II)-Pro, Cu(II)-His, Cu(II)-NA, pH 4, Cu(II)-NA, pH 7, and Cu(I/II)-glutathione. Pro was never detected as a ligand, as was the aquo complex. The data of Cu(II)-malate and Cu(II)-citrate were averaged like the data of Cu(II)-NA at pH 4 and 7. Left, Averaged samples of mature leaves from plants grown on 10 μM Zn^{2+} and 100 μM Cd^{2+}: Cd-K edge (data from Küpper et al., 2004). Plant x-ray absorption spectra were fitted with a linear combination of the EXAFS spectra of the following model compounds: aqueous ($CdSO_4$), Cd(II)-malate, Cd(II)-citrate, Cd(II)-His, and Cd(II)-glutathione. The data of Cd(II)-malate, Cd(II)-citrate, and the aquo complex were averaged. Similar results as for Cd were obtained for Zn; see Küpper et al. (2004).

leaf layers. The stronger decrease of Φ_{PSII} compared with F_v/F_m indicates the presence of a second inhibition target in addition to the inactivation of PSII reaction centers, such as inhibition of electron transfer after PSII or inhibition of the water-splitting complex as postulated earlier. The increasing light saturation under Cu stress observed now indicates that in a system of high antenna connectivity, the number of functional PSII reaction centers decreases faster than the number of functional antenna complexes; similar effects were observed for Cd stress in *T. caerulescens* (Küpper et al., 2007a). While under Cd stress, however, the nonphotochemical quenching of excitation energy increased, and Cu stress led to negative values of NPQ [$(F_m - F_m')/F_m$]. Such negative NPQ values, meaning that maximal fluorescence quantum yield is larger in the light-acclimated state than in the dark-acclimated state, are possible only if an increase of the PSII-associated antenna occurs in response to light. Hence, it may be concluded that Cu causes enhanced state I transitions (i.e. migration of LHCII from PSI to PSII). This makes sense if the second point (besides the PSII reaction center) in the inhibition of photochemistry is an inhibition of the water-splitting complex. Such an inhibition would result in a strongly oxidized plastoquinone pool, since PSII could "pump" as many electrons into it as PSI takes out of it, and an oxidized plastoquinone pool is well known to induce state I transitions.

All Cu toxicity-induced effects discussed above were milder in the few Cu-resistant compared with the normal Cu-sensitive individuals of *T. caerulescens*. Interestingly, the less severe reduction of F_v/F_m and Φ_{PSII} was only partially caused by a lesser increase of F_0 but also by a stronger increase of F_m in the resistant compared with the sensitive individuals. This indicates that the resistance involved not only a better Cu detoxification (see discussion of Cu ligands below) but also an enhanced repair of Chl-protein complexes.

Cu Ligands in *T. caerulescens*

Metallothioneins

Clearly, a strong contribution of S ligands to binding of Cu was found in most of the samples. In view of a generally very high expression of metallothioneins in *T. caerulescens* (Papoyan and Kochian, 2004), it is most likely that this S binding at least partially originates from Cu(I)-S clusters in metallothioneins. Already, previous studies indicated that in plants metallothioneins are much more relevant for Cu homeostasis than for Zn homeostasis (Cobbett and Goldsbrough, 2002), and physiological studies suggested a role for them in *T. caerulescens* (Roosens et al., 2004). Furthermore, Cu (I) metallothioneins are known to form very rigid Cu-S clusters that stabilize Cu(I) in aqueous solution (Byrd et al., 1988; Cobine et al., 2004). Strong multiple scattering due to this rigid structure is to be expected (Calderone et al., 2005) and might contribute to the EXAFS peaks at 2.7 Å and at 3.7 Å (George et al., 1988; Sayers et al., 1993). A contribution from metallothioneins would further explain why the XANES (the x-ray absorption close to the K edge) of our spectra shows a clear contribution of monovalent

Table IV. *Results of the refinement (explanation with a theoretical model) of the EXAFS spectra of plant samples using the DL-Excurve program*

To obtain representative data sets within the limited synchrotron beamtime, aliquots of samples from all similarly aged leaves of the same plant were mixed. When available, leaves of several individuals from the same experiment with similar Cu resistance were mixed as well. EF, Fermi energy, defines the threshold for the EXAFS spectra (Rehr and Albers, 2000); FI, fit index, increases with decreasing quality of the fit; SE, mathematical SE values of the refinement (2σ level). The error of the EXAFS approach as such is higher; this is revealed by the differences between samples of the same type. Asterisks ($*^1$, $*^2$, *) indicate values that were constrained to be identical for these contributions. Deviations from this simplification do not improve the model significantly. The amplitude reduction factor (Rehr and Albers, 2000) was set to 0.75. For NA, the structural model obtained in the refinement of the model complex has been used, keeping the metal C distances constant and defining their DW factors to 120% of the corresponding first shell value.

Sample, Including No. of Individual Plants Used to Prepare It	No., Type of Ligands ± SE	Distance ± SE	$2\sigma_i^2 \pm 2\sigma$ SD	EF ± SE	FI
		Å	$Å^2$	*eV*	k^3
Resistant individual, young leaves, first sample	1.6 ± 0.4, S	2.279 ± 0.015	0.004 ± 0.003*[1]	−7.0 ± 2.0	1.710
	0.1 ± 1.1, O	1.962 ± 0.021*	0.004 ± 0.003*[1]		
	2.2 ± 1.7, NA	1.962 ± 0.021*	0.004 ± 0.003*[1]		
	2.5 (±1.7), P	2.825 ± 0.023	0.011 ± 0.010		
	1.4 ± 0.7, Cu	3.388 ± 0.017	0.004 ± 0.005*[2]		
	0.8 ± 0.8, Cu	4.333 ± 0.046	0.004 ± 0.005*[2]		
	6.1 ± 3.3, Cu	5.207 ± 0.016	0.004 ± 0.005*[2]		
Two resistant individuals, young leaves, second sample[a]	2.0 ± 0.3, S	2.289 ± 0.010	0.011 ± 0.002*[1]	−6.9 ± 1.3	0.773
	0.1 ± 1.5, O	1.932 ± 0.022*	0.011 ± 0.002*[1]		
	2.3 ± 1.7, NA	1.932 ± 0.022*	0.011 ± 0.002*[1]		
	3.2 ± 0.9, P	2.738 ± 0.009	0.010 ± 0.004		
	0.5 ± 0.2, Cu	3.637 ± 0.024	0.004 ± 0.002*[2]		
	1.3 ± 0.4, Cu	4.391 ± 0.016	0.004 ± 0.002*[2]		
	3.4 ± 0.3, Cu	5.212 ± 0.012	0.004 ± 0.002*[2]		
Two resistant individuals, young leaves, third sample	1.4 ± 0.3, S	2.286 ± 0.011	0.004 ± 0.003*[1]	−8.7 ± 1.5	1.213
	1.7 ± 0.5, O	1.947 ± 0.013*	0.004 ± 0.003*[1]		
	0.2 ± 0.6, NA	1.947 ± 0.013*	0.004 ± 0.003*[1]		
	2.0 ± 1.0, P	2.848 ± 0.016	0.007 ± 0.007		
	1.0 ± 0.6, Cu	3.365 ± 0.016	0.004 ± 0.005*[2]		
	1.2 ± 0.8, Cu	4.376 ± 0.023	0.004 ± 0.005*[2]		
	4.1 ± 2.0, Cu	5.200 ± 0.013	0.004 ± 0.005*[2]		
Resistant individual, mature leaves, first sample[a]	1.1 ± 0.2, S	2.307 ± 0.012	0.009 ± 0.002*[1]	−12.3 ± 0.9	1.071
	0.1 ± 0.3, O	1.945 ± 0.011*	0.009 ± 0.002*[1]		
	2.5 ± 0.4, NA	1.945 ± 0.011*	0.009 ± 0.002*[1]		
	0.7 ± 0.6, P	3.023 ± 0.020	0.004 ± 0.010		
	0.3 ± 0.3, Cu	3.668 ± 0.033	0.004 ± 0.006*[2]		
	0.1 ± 0.3, Cu	4.379 ± 0.151	0.004 ± 0.006*[2]		
	2.5 ± 1.7, Cu	5.233 ± 0.011	0.004 ± 0.006*[2]		
Four resistant individuals, mature leaves, second sample	2.1 ± 0.4, S	2.245 ± 0.008	0.006 ± 0.003*[1]	−7.2 ± 1.4	0.972
	0.1 ± 1.8, O	1.912 ± 0.037*	0.006 ± 0.003*[1]		
	1.6 ± 2.1, NA	1.912 ± 0.037*	0.006 ± 0.003*[1]		
	1.0 ± 0.9, P	2.819 ± 0.019	0.004 ± 0.008		
	0.6 ± 0.3, Cu	3.705 ± 0.034	0.004 ± 0.002*[2]		
	2.9 ± 0.5, Cu	4.389 ± 0.011	0.004 ± 0.002*[2]		
	3.7 ± 1.0, Cu	5.216 ± 0.012	0.004 ± 0.002*[2]		
Sensitive individual, young leaves, first sample[a]	1.4 ± 0.2, S	2.275 ± 0.008	0.006 ± 0.002*[1]	−9.5 ± 0.9	0.710
	1.9 ± 0.8, O	1.933 ± 0.011*	0.006 ± 0.002*[1]		
	0.6 ± 0.9, NA	1.933 ± 0.011*	0.006 ± 0.002*[1]		
	1.0 ± 0.5, P	2.871 ± 0.017	0.004 ± 0.006		
	0.7 ± 0.6, Cu	3.719 ± 0.092	0.011 ± 0.008*[2]		
	0.8 ± 1.0, Cu	4.347 ± 0.045	0.011 ± 0.008*[2]		
	3.7 ± 2.5, Cu	5.229 ± 0.042	0.011 ± 0.008*[2]		
Two sensitive individuals, mature leaves, second sample[a]	1.1 ± 0.2, S	2.255 ± 0.008	0.006 ± 0.002*[1]	−8.6 ± 1.3	0.876
	0.1 ± 0.3, O	1.907 ± 0.027*	0.006 ± 0.002*[1]		
	2.5 ± 0.4, NA	1.907 ± 0.027*	0.006 ± 0.002*[1]		
	0.7 ± 0.6, P	2.872 ± 0.043	0.005 ± 0.010		
	0.3 ± 0.3, Cu	3.306 ± 0.036	0.009 ± 0.008*[2]		
	0.1 ± 0.3, Cu	4.386 ± 0.020	0.009 ± 0.008*[2]		
	2.5 ± 1.7, Cu	5.238 ± 0.033	0.009 ± 0.008*[2]		

(*Table continues on following page.*)

Table IV. (*Continued from previous page.*)

Sample, Including No. of Individual Plants Used to Prepare It	No., Type of Ligands ± SE	Distance ± SE	$2\sigma_i^2 \pm 2\sigma$ SD	EF ± SE	FI
Five sensitive individuals, young-mature leaves, third sample	0.4 ± 0.2, S	2.333 ± 0.027	0.007 ± 0.002*[1]	−9.2 ± 0.8	0.747
	0.1 ± 0.7, O	1.958 ± 0.008*	0.007 ± 0.002*[1]		
	3.6 ± 0.8, NA	1.958 ± 0.008*	0.007 ± 0.002*[1]		
	0.3 ± 0.3, P	2.951 ± 0.047	0.004 ± 0.012		
	0.4 ± 0.3, Cu	3.659 ± 0.026	0.004 ± 0.005*[2]		
	0.1 ± 0.3, Cu	4.366 ± 0.151	0.004 ± 0.005*[2]		
	3.0 ± 1.7, Cu	5.217 ± 0.010	0.004 ± 0.005*[2]		

[a]Shown in Figure 5.

Cu despite the high O content in plant tissues. All of these indications of a metallothionein contribution were much more pronounced in the Cu-resistant compared with the Cu-sensitive individuals of *T. caerulescens*.

Biomineralization

Modeling our EXAFS spectra with contributions from metallothioneins could explain the S contribution to the first ligand shell and possibly Cu-Cu interactions at 2.7 Å and 3.7 Å. But it does not explain the other contributions (e.g. the strong peaks at about 4.4 and 5.2 Å). Like the metallothioneins, the latter two contributions occurred in particular in the more Cu-resistant individuals of *T. caerulescens* and could be identified for all samples. Their high intensity (in particular the 5-Å peak) suggests that it is a metal-metal interaction, because lighter elements cannot result in such a large peak at such an extreme distance from the central atom. Even multiple scattering within the first shell that recently has been identified in a very limited number of metalloproteins (Ha et al., 2007; Hollenstein et al., 2009) would occur at shorter distances and thus can be ruled out. The identity of the metal at 5 Å can be obtained from the EXAFS data only with an uncertainty of one or two atomic numbers, but due to the metal content in the plant samples it could only be a Cu-Cu interaction. Comparing our data with the literature showed a striking similarity of these and other scattering peaks found in our samples with Cu moolooite, a hydrated crystalline form of Cu oxalate. EXAFS of Cu oxalate was described already by Michalowicz et al. (1979) and was first described as a naturally occurring mineral, moolooite, by Clarke and Williams (1986). Soon after, it was detected to occur in Cu-tolerant lichens (Chisholm et al., 1987; confirmed by Purvis et al., 2008), and recently it was shown (by Cu-EXAFS) to be formed by the highly heavy metal-tolerant fungus *Beauvaria caledonica* (Fomina et al., 2005). The Cu-EXAFS spectra published by the latter authors clearly showed all characteristic peaks of Cu-moolooite in the fungal "biominerals." In our own data, qualitatively all contributions to be expected from Cu-moolooite were present as well. The 5-Å peak, however, was often much higher (relative to the other contributions) in our samples than what could be expected from the spectrum of Cu-moolooite. Therefore, it cannot be excluded that another substance contributed to the 5-Å Cu-Cu interactions in *T. caerulescens*. Only a few compounds are known to have a high contribution at such an extreme distance from the central atom. Candidates are a Cu oxide, CuO, also known as the mineral tenorite (EXAFS spectrum published by Zhou et al., 1999), and hydrocalcite (EXAFS spectrum published by Porta et al., 1996). Features similar to the ones observed in our *T. caerulescens* samples were reported for samples collected from *L. tridentata* in its natural environment (Polette et al., 2000), but at that time no reference compounds with similar Cu-EXAFS spectrum were known. Therefore, these authors called this Cu speciation "unknown," with an assumption based on non-EXAFS data about bond distances that the 3.7-Å peak in the EXAFS spectrum may be attributed to Cu-Cu interactions in chalcopyrite. Furthermore, as their samples were collected in the natural environment and contained Cu-rich dust particles inside the stomatal cavities, in their case this Cu mineral was not due to biomineralization. In our case, such deposits of dust from Cu minerals can be excluded, as our plants were raised in a growth chamber on hydroponic solution. Revealing the exact identity of the Cu clusters that give rise to the extremely intense features in the EXAFS spectra of *T. caerulescens* will be an exciting but challenging task for future research.

NA

Most of the remainder of the higher shell contributions, in particular the peak at 2.7 to 3 Å, seems to be due to Cu binding to the nonproteogenic amino acid NA, which has been shown to have a very high affinity for Cu (Beneš et al., 1983), and already earlier works suggested, on a physiological basis, that NA is involved in Cu homeostasis (Pich and Scholz, 1996; Liao et al., 2000; Irtelli et al., 2009). The explanation of the features in our EXAFS spectra with carboxylate-bound NA seems more likely than the explanation by His, as seen by the statistical analysis of the fits. Because of the finding that NA plays a role in Cu binding in *T.*

caerulescens, we further characterized this ligand in isolated form. The combination of EXAFS and EPR data of Cu(II)-NA showed that Cu(II) was coordinated in a hexadentate way, with four short-distance and two long-distance ligands. This is in agreement with the structure of the mugeinic acid model from Nomoto et al. (1981). Titration indicated that only above pH 4 does Cu bind to the carboxyl groups of NA. The UV/VIS absorption and EPR spectra at different pH values, however, strongly change already above pH 3. Also, the Cu-NA EXAFS spectra at pH 4 and 7 yielded similar results, showing the scattering pattern typical for NA. Obviously, the latter methods are better in detecting the beginning of the Cu binding to NA, where the interaction is not yet strong enough to influence the pH value.

Summary of Cu Complexation Strategies in T. caerulescens

The finding of strong contributions from S ligands and from the tightly binding amino acid NA, as well as the discovery of Cu clusters that strongly suggest the occurrence of Cu biomineralization in *T. caerulescens*, were surprising in view of our earlier study (Küpper et al., 2004) on ligands of the hyperaccumulated Cd and Zn in the same species. That study had shown that in these plants Zn and even the normally S ligand-bound Cd is bound by weak O/N ligands. The new finding of predominantly strong ligands around Cu indicates that hyperaccumulators have completely different strategies of detoxification for metals that are hyperaccumulated (in this case, Cd and Zn) compared with nonhyperaccumulated metals (Cu). For the hyperaccumulated metals, detoxification is mainly based on active sequestration into the vacuoles of the epidermis, where they are stored only loosely associated with organic acids that are anyhow abundant in this organelle. Strong ligands like the phytochelatins and metallothioneins that detoxify heavy metals in nonaccumulator plants do not play a major role in the detoxification of hyperaccumulated metals in hyperaccumulator plants. This view was now reinforced also by our companion study (Küpper et al., 2009) on Cu metabolism in *C. helmsii*, where Cu was bound exclusively by weak O ligands (most likely organic acids such as malate). In contrast, it seems that hyperaccumulators deal with nonaccumulated metals in the same way as nonaccumulator plants (i.e. by binding them with strong ligands like metallothioneins and NA). In addition, strong indications were found for a detoxification of Cu by biomineralization. These forms of Cu detoxification, in particular metallothioneins and biomineralization, are clearly enhanced in the Cu-resistant compared with the Cu-sensitive *T. caerulescens* individuals. Therefore, phytoremediation of soils with mixed contamination including Cu could most likely be improved (compared with the normal wild-type population of the Ganges ecotype) by selective breeding of the Cu-tolerant *T. caerulescens* individuals.

MATERIALS AND METHODS

Plant Material, Culture Media, and Culture Conditions

Seeds of *Thlaspi caerulescens* (Ganges population), *Thlaspi fendleri*, and *Thlaspi ochroleucum* were germinated on a mixture of perlite and vermiculite moistened with deionized water. Three weeks after germination, seedlings were transferred to a nutrient solution containing 1,000 μM $Ca(NO_3)_2$, 500 μM $MgSO_4$, 50 μM K_2HPO_4, 100 μM KCl, 10 μM H_3BO_3, 0.1 μM $MnSO_4$, 0.2 μM Na_2MoO_4, 0.1 μM $CuSO_4$, 0.5 μM $NiSO_4$, 20 μM Fe(III)-ethylenediamine-di(*o*-hydroxyphenylacetic acid) [Fe(III)-EDDHA], and 10 μM $ZnSO_4$ (i.e. as in Shen et al., 1997, but with lower Cu and manganese). The pH of the solution was maintained at around 6.0 with 2.0 mM MES (pH adjustment with KOH). As in many previous studies (Küpper et al., 1999, 2004, 2007a, 2007b; Lombi et al., 2000), the nutrient solution contained 10 μM Zn because of the high Zn requirement of Zn hyperaccumulators (Shen et al., 1997). The nutrient solution was aerated continuously. After 12 $\pm$ 2 d of growth, 10 μM Cu^{2+} (as $CuSO_4$) was added to half of the pots. We used this concentration because initial tests had shown that it is sublethally toxic to both species investigated in our two companion studies, *Crassula helmsii* (Küpper et al., 2009) and *T. caerulescens* (this article). Using more Cu concentrations was impossible for practical reasons like measuring time at the FKM and beamtime at the synchrotron (almost 1 month already, which is longer than most other studies are allowed to take). We used a higher (but still sublethal) Cu concentration than Benzarti et al. (2008) for better comparability with *C. helmsii* and because otherwise the Cu concentration in the *T. caerulescens* plants would have remained below the detection limit of EXAFS; already under our conditions we needed 3 d of synchrotron measuring time per sample. At half the concentration in the tissue, it would have been about 12 d for the same signal-noise ratio, making the measurement of sufficient replicates impossible even when working with only one Cu concentration, as explained above. Furthermore, we grew the plants for 4 months rather than 5 d as in the study of Benzarti et al. (2008), because we wanted to investigate the long-term responses of the plant as these are more relevant than short-term toxicity for survival of the plant and for phytoremediation purposes. All chemicals except the EDDHA were analytical grade and purchased from Merck (www.merck.de); Fe(III)-EDDHA was purchased from Duchefa Biochemie (www.duchefa.com).

This study altogether lasted for 9 years (2000–2009), and the experiments were carried out in two blocks with the development of a new FKM and data analysis in between. Altogether, Cu stress + acclimation was investigated in seven experiments. In our first two experiments that included Cu treatments of *T. caerulescens* (2000–2001; data analysis 2001–2003), we used 1.5-L vessels with three to four plants each and renewed the solutions manually every 4 d (i.e. renewal rate per plant about 85 mL d^{-1}). In the second series (five experiments, 2004–2006; data analysis 2007–2009), we used 6-L vessels with seven plants each, in which the solution was exchanged continuously (1,700 mL d^{-1} per pot, i.e. 250 mL d^{-1} per plant) with the programmable 24-channel peristaltic pump "MCP process" (Ismatec; www.ismatec.com). The solutions in the pots were constantly thoroughly mixed via a laboratory-built medium injection system (Küpper et al., 2007a). The increased flow rate in the second experiment series was chosen to make sure that Cu uptake into the plants was not limited by the total amount available in the solution but only by the concentration. While for Cd in *T. caerulescens* this yielded stronger stress compared with the earlier experiments (Küpper et al., 2007a), showing that Cd toxicity was limited by the total Cd per pot due to hyperaccumulation in the plants, for Cu we did not observe a measurable difference between the high and low flow rates in the second versus the first experiment series.

All plants were grown with a 14-h daylength. In the first series of experiments, 24°C/20°C day/night temperature and a constant irradiance of 60 μE (from a 1:1 mixture of cool-white and Fluora fluorescent tubes; OSRAM; www.osram.com) during the light period were applied. In the second series, 22°C/18°C day/night temperature was applied and a quasisinusoidal three-step light cycle with about 40 μE in the morning and 120 μE at noon was achieved by full-spectrum discharge lamps.

Despite the differences in growth conditions between the first and second series of experiments, all trends of changes in photosynthetic parameters and growth were found in both series, so that all experiments are analyzed together in "Results" and "Discussion."

Chl Fluorescence Kinetic Measurements

These were done with the FKM (developed by Küpper et al., 2000b, 2007a) as described in the companion article (Küpper et al., 2009) on *C. helmsii*, except

for keeping the leaves in water-saturated air. To perform a measurement, a leaf was cut off and pressed by its upper side (for palisade mesophyll measurements) or lower side (for spongy mesophyll measurements) toward the glass window of the measuring chamber with a wet nylon grid or wet cellophane. The chamber was ventilated by a stream of water-saturated air (2 L min^{-1}, 21°C). The construction and operation of the chamber are in principle as described by Küpper et al. (2000b); the new version is shown by Küpper et al. (2007a). All measurements were done on the mesophyll away from the veins.

Analysis of Fluorescence Kinetics

The original data (i.e. two-dimensional records of Chl fluorescence kinetics) were analyzed using FluorCam6 software from Photon Systems Instruments as described earlier (Küpper et al., 2000b, 2007a) and in our companion article (Küpper et al., 2009) on *C. helmsii*. All parameters of fluorescence kinetics used in this study are explained in Table I; a more detailed description of the technique as such and of all basic parameters can be found in the review by Maxwell and Johnson (2000).

Preparation of Plant Samples for EXAFS Measurements

EXAFS samples were taken during the second series of experiments (see above). After about 6 months of plant growth, samples were taken from leaves of several developmental stages. To eliminate problems of element redistribution during sample preparation, the collected tissues were shock frozen in melting N slush. This slush was generated by pulling a strong vacuum on a container of well-insulated liquid nitrogen (this forces the N into a solid + gaseous state) and then releasing the vacuum, causing the N "snow" to melt. This rapid freeze method prevents, in contrast to liquid nitrogen, the formation of a gas layer that slows freezing of the sample. Afterward, samples were immediately stored at –80°C. To obtain representative data sets within the limited synchrotron beamtime, aliquots of samples from all plants of the same metal treatment (see above) were mixed, so that each EXAFS sample represented the average of more than 10 plants. For the EXAFS measurements, the frozen-hydrated samples were ground to powder in a mortar and filled into EXAFS cuvettes; all this was done at –80°C (dry ice cooling). Afterward, the cuvettes were sealed with Kapton tape and stored in liquid nitrogen.

Preparation of Cu Complexes for Spectroscopic Measurements

A 5 mM solution of $CuSO_4$ in water was used as reference for the aquo complex. His, citrate, and glutathione complexes were made by adding 50 mM ligand to a 5 mM $CuSO_4$ solution in water. Our citrate and aquo complexes were acidic, adjusted to pH 4, resembling the situation in plant vacuoles, which are the compartments where plants store organic acids and which are the main sinks for heavy metals in hyperaccumulators (Küpper et al., 1999, 2001). The His and glutathione complexes were prepared both at pH 4 and pH 7. Samples of Cu(II)-NA were prepared by potentiometric titration of a solution of 2.5 mM ligand and 2 mM $CuCl_2$ in water under the exclusion of dioxygen (N atmosphere). Aliquots of 0.1 M KOH were added stepwise to reach pH 11. Samples for UV/VIS and EPR spectroscopy were taken at pH 2, 3, 4, 5, 6, 7, 8, 9, 10, and 11; samples for EXAFS spectroscopy were taken at pH 4 and 7. Thereafter, the solution was titrated back from pH 11 to pH 2 with 0.1 M HCl. For EXAFS and EPR spectroscopy, 10% (v/v) glycerol was added to all solutions of the model complexes to minimize the formation of ice crystals during freezing. Those samples were transferred into EXAFS cuvettes and frozen in liquid nitrogen or into EPR tubes and frozen in supercooled (−140°C) isopentane.

EXAFS Measurements and Data Analysis

Measurements were performed at the EMBL bending magnet beamline D2 (DESY) using a Si(111) double crystal monochromator, a focusing mirror, and a 13-element germanium solid-state fluorescence detector. All samples were mounted in a top-loading closed-cycle cryostat (modified from Oxford Instruments) and kept at about 30 K. The transmitted beam was used for energy calibration by means of the Bragg reflections of a static Si(220) crystal (Pettifer and Hermes, 1985). At least 500,000 counts above the Cu-K absorption edge were accumulated for each measurement. Data reduction and averaging were done using the EXPROG (Korbas et al., 2006) and KEMP (Korbas et al., 2006) packages of programs. Data analysis was performed using DL_Excurv (Tomic et al., 2005), which is a freeware version of Excurve (Binstead et al., 1992) under the flagship of CCP3 (www.ccp3.ac.uk/).

The k-range was chosen according to the statistical quality of the data at the end of the k-range, from 3 $Å^{-1}$ to a higher end at 8.5 to 13 $Å^{-1}$. In doubtful cases, the fits were performed in an extended and a shortened k-range, in order to test the significance of the low scattering contributions in the fit. Since N and O are indistinguishable by EXAFS due to their similar scattering phases, both elements are used indistinctively. But multiple scattering contributions (e.g. of the imidazole ring of His) may allow unambiguous assignment of ligand molecules (e.g. His, NA). Several models were attempted for the refinement, with different coordination numbers and mixtures of ligands in the first shell. The individual contributions of the potential ligands were floated during the refinement; in this way, the possibility of several Cu species was tested. In the cases where scattering contributions were seen beyond the first shell, mixed first shells including His, NA, and other low-Z ligands (N/O) were tried. For explaining the contributions at long distances from the central atom, many models were tried, as described in "Results." Comparison with a Cu foil spectrum indicated that artifacts of contaminating scattered photons from the cryostat Cu should have been minimal. Trying to refine such a contribution led only to very low percentages (usually less than 5% of total Cu). In addition, the intensity of the 5-Å peak was highest in samples with rather high Cu content (i.e. the resistant specimens), while the contribution from cryostat reflections should have been strongest in samples low in internal Cu. This was reproducibly found in 2 measuring years.

His was modeled using the coordinates provided by the DL-Excurve release. The NA coordinates were taken from NICOAM01.cif (Miwa et al., 1999). The initial NA structure was taken from Nomoto et al. (1981). The Cu model compound of Nomoto et al. (1981) is 6-coordinated, with two longer Cu ligand bonds. For the phase calculations of NA, a metal site with a bound NA was built using Spartan Student Edition version 1.0.2 for Mac, with the ligand assumed to bind by the N on the plane of the ring and angles (Cu-N-C) of 121° with each neighboring C. In both cases, for His and NA rings, multiple scattering within the ring was included. Also, binding from the carboxyl groups of NA was included.

In addition to the EXAFS refinement, as in our previous study on Cd and Zn ligands in *T. caerulescens* (Küpper et al., 2004) we used a fit with a linear combination of all measured model complexes (aqueous, malate, citrate, NA, His, Pro, glutathione) as an independent way to determine the proportions of ligand types binding the Cu in plant tissues. This fit is subsequently called "component analysis." The fitting of measured x-ray absorption spectra sample data by a linear combination of measured model data has also successfully been used by Salt et al. (1999) for Zn in samples of *T. caerulescens*. In this work, the approach of Salt et al. (1999) was modified as described by Küpper et al. (2004).

Determination of Metals in Whole Plant Tissues

Frozen-hydrated plant samples (see above) were lyophilized, ground, and subsequently digested with a mixture of 85% (v/v) concentrated HNO_3 and 15% (v/v) concentrated $HClO_4$ (Zhao et al., 1994). Concentrations of Cu in the digests were determined using atomic absorption spectrometry in a GBC 932 AA spectrometer (GBC Scientific Equipment).

UV/VIS Spectroscopy and Pigment Analysis

UV/VIS spectra were measured with the double beam spectrometer Lambda 16 (Perkin-Elmer; las.perkinelmer.com) at 22°C ± 2°C with a scanning speed of 240 nm min^{-1}. An optical path length of 10 mm, a 1-nm spectral bandwidth, and a 0.2-nm sampling interval were selected for all measurements. For pigment quantification, leaves were frozen in liquid nitrogen, then lyophilized, and finally extracted in 100% acetone. Chls and carotenoids were quantified according to Küpper et al. (2007c) as described in detail in our companion article (Küpper et al., 2009) on *C. helmsii*.

EPR Spectroscopy

EPR spectra (perpendicular mode, X-band) were recorded on a Bruker Elexsys 500 with an ER 049 X microwave bridge (Bruker BioSpin; http://www.bruker-biospin.com). The system was equipped with an Oxford Instruments ESR 900 helium cryostat controlled by the ITC 503 temperature device. The modulation frequency was 100 kHz, and the modulation amplitude was typically 0.1 mT. The measurements were performed with a Bruker 4122

SHQE cavity at approximately 9.34 GHz. The microwave power was adjusted to obtain maximum signal intensity at the given temperature of 20 K. Sample tubes were Suprasil quartz tubes 705-PQ-9.50 (Wilmad) with an o.d. of 4 mm and sample volume of 250 μL. Samples were frozen in liquid nitrogen and kept at 77 K. Spectra were evaluated with Xepr software (Bruker), and $CuSO_4$ in 2 M $NaClO_4$/HCl, pH 1.5, served as the standard for quantitation.

ACKNOWLEDGMENT

We are very grateful to Ivan Šetlík for stimulating discussions about interpretation of the fluorescence kinetic parameters.

Received July 12, 2009; accepted August 12, 2009; published August 19, 2009.

LITERATURE CITED

Ascone I, Meyer-Klaucke W, Murphy L (2003) Experimental aspects of biological x-ray absorption spectroscopy. J Synchrotron Radiat **10:** 16–22

Assunção AGL, Costa Martins PDA, De Folter S, Vooijs R, Schat H, Aarts MGM (2001) Elevated expression of metal transporter genes in three accessions of the metal hyperaccumulator *Thlaspi caerulescens*. Plant Cell Environ **24:** 217–226

Assunção AGL, Schat H, Aarts MGM (2003) Thlaspi caerulescens, an attractive model species to study heavy metal hyperaccumulation in plants. New Phytol **159:** 351–60

Becher M, Talke IN, Krall L, Krämer U (2004) Cross-species microarray transcript profiling reveals high constitutive expression of metal homeostasis genes in shoots of the zinc hyperaccumulator *Arabidopsis halleri*. Plant J **37:** 251–268

Beneš I, Schreiber K, Ripperger H, Kircheiss A (1983) Metal complex formation by nicotianamine, a possible phytosiderophore. Experientia **39:** 261–262

Benzarti S, Mohri S, Ono Y (2008) Plant response to heavy metal toxicity: comparative study between the hyperaccumulator Thlaspi caerulescens (ecotype Ganges) and nonaccumulator plants: lettuce, radish, and alfalfa. Environ Toxicol **23:** 607–616

Bidwell SD, Crawford SA, Woodrow IE, Summer-Knudsen J, Marshall AT (2004) Sub-cellular localization of Ni in the hyperaccumulator, *Hybanthus floribundus* (Lindley) F. Muell. Plant Cell Environ **27:** 705–716

Binstead N, Strange RW, Hasnain SS (1992) Constrained and restrained refinement in EXAFS data analysis with curved wave theory. Biochemistry **31:** 12117–12125

Broadhurst CL, Chaney RL, Angle JS, Erbe EF, Maugel TK (2004) Nickel localization and response to increasing Ni soil levels in leaves of the Ni hyperaccumulator *Alyssum murale*. Plant Soil **265:** 225–242

Brooks RR (1998) Geobotany and hyperaccumulators. *In* RR Brooks, ed, Plants That Hyperaccumulate Heavy Metals. CAB International, Wallingford, UK, pp 55–94

Byrd J, Berger RM, McMillin DR, Wright CF, Hamer D, Winge DR (1988) Characterization of the copper-thiolate cluster in yeast metallothionein and two truncated mutants. J Biol Chem **263:** 6688–6694

Calderone V, Dolderer B, Hartmann HJ, Echner H, Luchinat C, Del Bianco C, Mangani S, Weser U (2005) The crystal structure of yeast copper thionein: the solution of a long-lasting enigma. Proc Natl Acad Sci USA **102:** 51–56

Callahan DL, Baker AJM, Kolev SD, Wedd AG (2006) Metal ion ligands in hyperaccumulating plants. J Biol Inorg Chem **11:** 2–12

Chisholm JE, Jones GC, Purvis OW (1987) Hydrated copper oxalate, moolooite, in lichens. Mineral Mag **51:** 715–718

Clarke RM, Williams IR (1986) Moolooite, a naturally occurring hydrated copper oxalate from Western Australia. Mineral Mag **50:** 295–298

Cobbett C, Goldsbrough P (2002) Phytochelatins and metallothioneins: roles in heavy metal detoxification and homeostasis. Annu Rev Plant Biol **53:** 159–182

Cobine PA, McKay RT, Zangger K, Dameron CT, Armitage IM (2004) Solution structure of Cu6 metallothionein from the fungus Neurospora crassa. Eur J Biochem **271:** 4213–4221

Ebbs S, Lau I, Ahner B, Kochian LV (2002) Phytochelatin synthesis is not responsible for Cd tolerance in the Zn/Cd hyperaccumulator *Thlaspi caerulescens* (J.&C. Presl). Planta **214:** 635–640

Fomina M, Hillier S, Charnock JM, Melville K, Alexander IJ, Gadd GM (2005) Role of oxalic acid overexcretion in transformations of toxic metal minerals by Beauveria caledonica. Appl Environ Microbiol **71:** 371–381

Frey B, Keller C, Zierold K, Schulin R (2000) Distribution of Zn in functionally different epidermal cells of the hyperaccumulator *Thlaspi caerulescens*. Plant Cell Environ **23:** 675–687

Gardea-Torresdey JL, Arteaga S, Tiemann KJ, Chianelli R, Pingitore N, Mackay W (2001) Absorption of copper(II) by creosote bush (Larrea tridentata): use of atomic and x-ray absorption spectroscopy. Environ Toxicol Chem **20:** 2572–2579

Genty B, Briantais J, Baker NR (1989) The relationship between the quantum yield of photosynthetic electron transport and quenching of chlorophyll fluorescence. Biochim Biophys Acta **990:** 87–92

George GN, Byrd J, Winge DR (1988) X-ray absorption studies of yeast copper metallothionein. J Biol Chem **263:** 8199–8203

Ha SW, Korbas M, Klepsch M, Meyer-Klaucke W, Meyer O, Svetlitchnyi V (2007) Interaction of potassium cyanide with the [Ni-4Fe-5S] active site cluster of CO dehydrogenase from Carboxydothermus hydrogenoformans. J Biol Chem **282:** 10639–10646

Hollenstein K, Comellas-Bigler M, Bevers LE, Feiters MC, Meyer-Klaucke W, Hagedoorn PL, Locher KP (2009) Distorted octahedral coordination of tungstate in a subfamily of specific binding proteins. J Biol Inorg Chem **14:** 663–672

Irtelli B, Petrucci WA, Navarri-Izzo F (2009) Nicotianamine and histidine/proline are, respectively, the most important copper chelators in xylem sap of Brassica carinata under conditions of copper deficiency and excess. J Exp Bot **60:** 269–277

Korbas M, Marsa DF, Meyer-Klaucke W (2006) KEMP: a program script for automated biological x-ray absorption spectroscopy data reduction. Rev Sci Instrum **77:** 063105

Küpper H, Aravind P, Leitenmaier B, Trtílek M, Šetlík I (2007a) Cadmium-induced inhibition of photosynthesis and long-term acclimation to Cd-stress in the Cd hyperaccumulator Thlaspi caerulescens. New Phytol **175:** 655–674

Küpper H, Götz B, Mijovilovich A, Küpper FC, Meyer-Klaucke W (2009) Complexation and toxicity of copper in higher plants. I. Characterization of copper accumulation, speciation, and toxicity in *Crassula helmsii* as a new copper accumulator. Plant Physiol **151:** 702–714

Küpper H, Kroneck PMH (2005) Heavy metal uptake by plants and cyanobacteria. *In* A Sigel, H Sigel, RKO Sigel, eds, Metal Ions in Biological Systems, Band 44, Kapitel 5. Marcel Dekker, New York, pp 97–142

Küpper H, Küpper F, Spiller M (1996) Environmental relevance of heavy metal substituted chlorophylls using the example of water plants. J Exp Bot **47:** 259–266

Küpper H, Küpper F, Spiller M (1998) In situ detection of heavy metal substituted chlorophylls in water plants. Photosynth Res **58:** 125–133

Küpper H, Lombi E, Zhao FJ, McGrath SP (2000a) Cellular compartmentation of cadmium and zinc in relation to other elements in the hyperaccumulator *Arabidopsis halleri*. Planta **212:** 75–84

Küpper H, Lombi E, Zhao FJ, Wieshammer G, McGrath SP (2001) Cellular compartmentation of nickel in the hyperaccumulators *Alyssum lesbiacum*, *Alyssum bertolonii* and *Thlaspi goesingense*. J Exp Bot **52:** 2291–2300

Küpper H, Mijovilovich A, Meyer-Klaucke W, Kroneck PMH (2004) Tissue- and age-dependent differences in the complexation of cadmium and zinc in the Cd/Zn hyperaccumulator *Thlaspi caerulescens* (Ganges ecotype) revealed by x-ray absorption spectroscopy. Plant Physiol **134:** 748–757

Küpper H, Seib LO, Sivaguru M, Kochian LV (2007b) A method for cellular localisation of gene expression via quantitative in situ hybridisation in plants. Plant J **50:** 159–187

Küpper H, Seibert S, Aravind P (2007c) A fast, sensitive and inexpensive alternative to analytical pigment HPLC: quantification of chlorophylls and carotenoids in crude extracts by fitting with Gauss-peak-spectra. Anal Chem **79:** 7611–7627

Küpper H, Šetlík I, Spiller M, Küpper FC, Prášil O (2002) Heavy metal-induced inhibition of photosynthesis: targets of in vivo heavy metal chlorophyll formation. J Phycol **38:** 429–441

Küpper H, Šetlík I, Trtilek M, Nedbal L (2000b) A microscope for two-dimensional measurements of *in vivo* chlorophyll fluorescence kinetics using pulsed measuring light, continuous actinic light and saturating flashes. Photosynthetica **38:** 553–570

Küpper H, Zhao FJ, McGrath SP (1999) Cellular compartmentation of zinc

in leaves of the hyperaccumulator *Thlaspi caerulescens*. Plant Physiol **119:** 305–311

Lanaras T, Moustakas M, Symeonidis L, Diamantoglou S, Karataglis S (1993) Plant metal content, growth responses and some photosynthetic measurements on field-cultivated wheat growing on ore bodies enriched in Cu. Physiol Plant **88:** 307–314

Lasat MM, Baker AJM, Kochian LV (1996) Physiological characterization of root Zn^{2+} absorption and translocation to shoots in Zn hyperaccumulator and nonaccumulator species of *Thlaspi*. Plant Physiol **112:** 1715–1722

Lasat MM, Baker AJM, Kochian LV (1998) Altered Zn compartmentation in the root symplasm and stimulated Zn absorption into the leaf as mechanisms involved in Zn hyperaccumulation in *Thlaspi caerulescens*. Plant Physiol **118:** 875–883

Liao MT, Hedley MJ, Woolley DJ, Brooks RR, Nichols MA (2000) Copper uptake and translocation in chicory (Cichorium intybus L. cv Grasslands Puna) and tomato (Lycopersicon esculentum Mill. cv Rondy) plants grown in NFT system. II. The role of nicotianamine and histidine in xylem sap copper transport. Plant Soil **223:** 243–252

Lombi E, Zhao FJ, Dunham SJ, McGrath SP (2000) Cadmium accumulation in populations of *Thlaspi caerulescens* and *Thlaspi goesingense*. New Phytol **145:** 11–20

Maxwell K, Johnson GN (2000) Chlorophyll fluorescence: a practical guide. J Exp Bot **51:** 659–668

Michalowicz A, Girerd JJ, Goulon J (1979) EXAFS determination of the copper oxalate structure: relation between structure and magnetic properties. Inorg Chem **18:** 3004–3010

Miwa Y, Mizuno T, Tsuchida K, Taga T, Iwata Y (1999) Experimental charge density and electrostatic potential in nicotinamide. Acta Crystallogr B **55:** 78–84

Nomoto K, Mino Y, Ishida T, Yoshioka H, Ota N, Inoue M, Takagi S, Takemoto T (1981) X-ray crystal-structure of the copper(II) complex of mugineic acid, a naturally-occurring metal chelator of graminaceous plants. J Chem Soc Chem Commun **7:** 338–339

Ouzounidou G, Moustakas M, Strasser RJ (1997) Sites of action of copper in the photosynthetic apparatus of maize leaves: kinetic analysis of chlorophyll fluorescence, oxygen evolution, absorption changes and thermal dissipation as monitored by photoacoustic signals. Aust J Plant Physiol **24:** 81–90

Papoyan A, Kochian LV (2004) Identification of *Thlaspi caerulescens* genes that may be involved in heavy metal hyperaccumulation and tolerance: characterization of a novel heavy metal transporting ATPase. Plant Physiol **136:** 3814–3823

Parameswaran A, Leitenmaier B, Yang M, Welte W, Kroneck PMH, Lutz G, Papoyan A, Kochian LV, Küpper H (2007) A native Zn/Cd transporting P1B type ATPase protein from natural overexpression in a Zn/Cd hyperaccumulator plant. Biochem Biophys Res Commun **364:** 51–56

Peer WA, Mahmoudian M, Freeman JL, Lahner B, Richards EL, Reeves RD, Murphy AS, Salt DE (2006) Assessment of plants from the Brassicaceae family as genetic models for the study of nickel and zinc hyperaccumulation. New Phytol **172:** 248–260

Peer WA, Mahmoudian M, Lahner B, Reeves RD, Murphy AS, Salt DE (2003) Development of a model plant to study the molecular genetics of metal hyperaccumulation. Part I. Germplasm analysis of 20 Brassicaceae accessions from Austria, France, Turkey, and USA. New Phytol **159:** 421–430

Pence NS, Larsen PB, Ebbs SD, Letham DLD, Lasat MM, Garvin DF, Eide D, Kochian LV (2000) The molecular physiology of heavy metal transport in the Zn/Cd hyperaccumulator *Thlaspi caerulescens*. Proc Natl Acad Sci USA **97:** 4956–4960

Pettifer RF, Hermes C (1985) Absolute energy calibration of x-ray radiation from synchrotron sources. J Appl Cryst **18:** 404–412

Pich A, Scholz I (1996) Translocation of copper and other micronutrients in tomato plants (Lycopersicon esculentum Mill.): nicotianamine-stimulated copper transport in the xylem. J Exp Bot **47:** 41–47

Pich A, Scholz G, Stephan UW (1994) Iron-dependent changes of heavy metals, nicotianamine, and citrate in different plant organs and in the xylem of two tomato genotypes: nicotianamine as possible copper translocator. Plant Soil **165:** 189–196

Pilon M, Abdel-Ghany SE, Cohu CM, Gogolin KA, Ye H (2006) Copper cofactor delivery in plant cells. Curr Opin Plant Biol **9:** 256–263

Polette LA, Gardea-Torresdey JL, Chianelli RR, George GN, Pickering IJ, Arenas J (2000) XAS and microscopy studies of the uptake and biotransformation of copper in Larrea tridentata (creosote bush). Microchem J **65:** 227–236

Porta P, Morpurgo S, Pettiti I (1996) Characterization by x-ray absorption, x-ray powder diffraction, and magnetic susceptibility of Cu-Zn-Co-Al-containing hydroxycarbonates, oxycarbonates, oxides, and their products of reduction. J Solid State Chem **121:** 372–378

Prasad MNV, Hagemeyer J, editors (1999) Heavy Metal Stress in Plants: From Molecules to Ecosystems. Springer, Berlin

Purvis OW, Pawlik-Skowronska B, Cressey G, Jones GC, Kearsley A, Spratt J (2008) Mineral phases and element composition of the copper hyperaccumulator lichen Lecanora polytropa. Mineral Mag **72:** 607–616

Rehr JJ, Albers RC (2000) Theoretical approaches to x-ray absorption fine structure. Rev Mod Phys **72:** 621–654

Roosens NH, Bernard C, Leplae R, Verbruggen N (2004) Evidence for copper homeostasis function of metallothionein (MT3) in the hyperaccumulator Thlaspi caerulescens. FEBS Lett **577:** 9–16

Sahi SV, Israra M, Srivastava AK, Gardea-Torresdey JL, Parsons JG (2007) Accumulation, speciation and cellular localization of copper in Sesbania drummondii. Chemosphere **67:** 2257–2266

Salt DE, Prince RC, Baker AJM, Raskin I, Pickering IJ (1999) Zinc ligands in the metal hyperaccumulator *Thlaspi caerulescens* as determined using x-ray absorption spectroscopy. Environ Sci Technol **33:** 712–717

Salt DE, Prince RC, Pickering IJ, Raskin I (1995) Mechanisms of cadmium mobility and accumulation in Indian mustard. Plant Physiol **109:** 1427–1433

Sayers Z, Brouillon P, Vorgias CE, Nolting HF, Hermes C, Koch MH (1993) Cloning and expression of Saccharomyces cerevisiae copper-metallothionein gene in Escherichia coli and characterization of the recombinant protein. Eur J Biochem **212:** 521–528

Schat H, Llugany M, Vooijs R, Hartley-Whitaker J, Bleeker PM (2002) The role of phytochelatins in constitutive and adaptive heavy metal tolerances in hyperaccumulator and nonhyperaccumulator metallophytes. J Exp Bot **53:** 2381–2392

Schmidke I, Stephan UW (1995) Transport of metal micronutrients in the phloem of castor bean (Ricinus communis) seedlings. Physiol Plant **95:** 147–153

Schünemann V, Meier C, Meyer-Klaucke W, Winkler H, Trautwein AX, Knappskog PM, Toska K, Haavik J (1999) Iron coordination geometry in full-length, truncated, and dehydrated forms of human tyrosine hydroxylase studied by Mössbauer and x-ray absorption spectroscopy. J Biol Inorg Chem **4:** 223–231

Shen ZG, Zhao FJ, McGrath SP (1997) Uptake and transport of zinc in the hyperaccumulator *Thlaspi caerulescens* and the non-hyperaccumulator *Thlaspi ochroleucum*. Plant Cell Environ **20:** 898–906

Shi J, Wu B, Yuan X, Cao YY, Chen X, Chen Y, Hu T (2008) An x-ray absorption spectroscopy investigation of speciation and biotransformation of copper in Elsholtzia splendens. Plant Soil **302:** 163–174

Stephan UW, Schmidke I, Stephan VW, Scholz G (1996) The nicotianamine molecule is made-to-measure for complexation of metal micronutrients in plants. Biometals **9:** 84–90

Stephan UW, Scholz G (1993) Nicotianamine: mediator of transport of iron and heavy metals in the phloem? Physiol Plant **88:** 522–529

Tomic S, Searle BG, Wander A, Harrison NM, Dent AJ, Mosselmans JFW, Inglesfield JE (2005) New Tools for the Analysis of EXAFS: The DL EXCURV Package. CCLRC Technical Report DL-TR-2005-001. Council for the Central Laboratory of the Research Councils, Swindon, UK

Ueno D, Ma JF, Iwashita T, Zhao FJ, McGrath SP (2005) Identification of the form of Cd in the leaves of a superior Cd-accumulating ecotype of Thlaspi caerulescens using 113Cd-NMR. Planta **221:** 928–936

van de Mortel JE, Almar Villanueva L, Schat H, Kwekkeboom J, Coughlan S, Moerland PD, Ver Loren van Themaat E, Koornneef M, Aarts MG (2006) Large expression differences in genes for iron and zinc homeostasis, stress response, and lignin biosynthesis distinguish roots of *Arabidopsis thaliana* and the related metal hyperaccumulator *Thlaspi caerulescens*. Plant Physiol **142:** 1127–1147

van de Mortel JE, Schat H, Moerland PD, Ver Loren van Themaat E, van der Ent S, Blankestijn H, Ghandilyan A, Tsiatsiani S, Aarts MG (2008) Expression differences for genes involved in lignin, glutathione and

sulphate metabolism in response to cadmium in Arabidopsis thaliana and the related Zn/Cd-hyperaccumulator Thlaspi caerulescens. Plant Cell Environ **31:** 301–324

von Wiren N, Klair S, Bansal S, Briat JF, Khodr H, Shioiri T, Leigh RA, Hider RC (1999) Nicotianamine chelates both FeIII and FeII: implications for metal transport in plants. Plant Physiol **119:** 1107–1114

Walker DJ, Bernal MP (2004) The effects of copper and lead on growth and zinc accumulation of Thlaspi caerulescens J. and C. Presl: implications for phytoremediation of contaminated soils. Water Air Soil Pollut **151:** 361–372

Weber M, Harada E, Vess C, von Roepenack-Lahaye E, Clemens S (2004) Comparative microarray analysis of *Arabidopsis thaliana* and *Arabidopsis halleri* roots identifies nicotianamine synthase, a ZIP transporter and other genes as potential metal hyperaccumulation factors. Plant J **37:** 269–281

Zhao F, McGrath SP, Crosland AR (1994) Comparison of three wet digestion methods for the determination of plant sulphur by inductively coupled plasma atomic emission spectrometry (ICP-AES). Commun Soil Sci Plant Anal **25:** 407–418

Zhou W, Hesterberg D, Hansen PD, Hutchison KJ, Sayers DE (1999) Stability of copper sulfide in a contaminated soil. J Synchrotron Radiat **6:** 630–632